Contactin Orchestrates Assembly of the Septate-like Junctions at the Paranode in Myelinated Peripheral Nerve

Mary E.T. Boyle,[1,5,6] Erik O. Berglund,[1,5]
Keith K. Murai,[1,2,5] Lynne Weber,[1,2]
Elior Peles,[3] and Barbara Ranscht[1,2,4]
[1] Neurobiology Program
The Burnham Institute
La Jolla, California 92037
[2] Department of Neuroscience
University of California, San Diego
La Jolla, California 92093
[3] Department of Molecular Cell Biology
The Weizmann Institute of Science
Rehovot 76100
Israel

Summary

Rapid nerve impulse conduction depends on specialized membrane domains in myelinated nerve, the node of Ranvier, the paranode, and the myelinated internodal region. We report that GPI-linked contactin enables the formation of the paranodal septate-like axo-glial junctions in myelinated peripheral nerve. Contactin clusters at the paranodal axolemma during Schwann cell myelination. Ablation of contactin in mutant mice disrupts junctional attachment at the paranode and reduces nerve conduction velocity 3-fold. The mutation impedes intracellular transport and surface expression of Caspr and leaves NF155 on apposing paranodal myelin disengaged. The contactin mutation does not affect sodium channel clustering at the nodes of Ranvier but alters the location of the Shaker-type Kv1.1 and Kv1.2 potassium channels. Thus, contactin is a crucial part in the machinery that controls junctional attachment at the paranode and ultimately the physiology of myelinated nerve.

Introduction

Intercellular junctions are instrumental in establishing membrane compartments with specialized functions in diverse cell types. One such junction is the septate-like junction at the paranode that flanks the node of Ranvier in myelinated nerve. This specialized axo-glial junction electrically isolates the myelinated from unmyelinated nerve segments and physically separates the voltage-gated sodium channels at the node from the cluster of potassium channels underneath the myelin sheath. This arrangement enables rapid saltatory propagation of action potentials from node to node (Brill et al., 1977; Bostock and Sears, 1978). The functionally distinct membrane compartments of myelinated nerve, including the node of Ranvier, the paranode, the juxtaparanode, and the internode, develop through an elaborate sequence

[4] Correspondence: ranscht@burnham.org
[5] These authors contributed equally to this work.
[6] Present address: University of California, San Diego, Cognitive Science Department, La Jolla, California 92093.

of cellular interactions between axons and myelin-forming glial cells. Schwann cells myelinate axons in the peripheral nervous system (PNS) and oligodendrocytes in the central nervous system (CNS) (Rosenbluth, 1984; Salzer, 1997). Both intrinsic factors as well as intercommunication between axons and glial cells are thought to contribute to the establishment of the specialized membrane domains in myelinated nerve (Kaplan et al., 1997; Lambert et al., 1997; Rasband et al., 1999).

In particular, the paranodal region has raised intriguing questions regarding the importance of axo-glial junctions with respect to nerve physiology. At the paranode, myelin loops terminate and engage in the formation of a septate-like adhesive junction with the axon membrane (Salzer, 1997; Peles and Salzer, 2000). This adhesive structure serves multiple functions. The paranodal junction constitutes the major site of attachment between the glial cell and the axon (Wiley and Ellisman, 1980; Ellisman et al., 1984; Rosenbluth, 1984). It also acts as an electrical and a biochemical barrier between nodal and internodal membrane compartments (Chiu and Ritchie, 1980; Barrett and Barrett, 1981; Funch and Faber, 1984; Rosenbluth, 1995). Furthermore, the paranodal junction is considered to be a conduit for molecular communication between the axon and the glial cell (Trapp and Kidd, 2000). Consistent with these multiple roles, the disruption of axo-glial contacts in myelinated nerve results in severe pathological conditions that have been characterized in a variety of mouse mutants (Rosenbluth, 1980, 1981, 1987; Wang et al., 1995). Thus, unraveling the molecular nature of axo-glial communication at the paranode will contribute significantly to the understanding of myelin dysfunction.

To date, relatively little is known about the molecular composition of the paranodal membrane specialization. One prominent component of the paranodal axolemma is Caspr (contactin-associated protein; also known as Paranodin), a transmembrane neurexin superfamily molecule with intra- and extracellular binding motifs for protein-protein and protein-carbohydrate interactions (Peles et al., 1997; Menegoz et al., 1997; Einheber et al., 1997). One group identified Caspr by nature of its *cis* interaction with the cell adhesion protein contactin (Peles et al., 1997), which is the subject of the current study. The apposing paranodal myelin membrane is demarcated by the immunoglobulin superfamily (IgSF) cell adhesion molecule neurofascin-155 (NF155) (Tait et al., 2000). This molecule can engage in *trans* binding interactions with contactin in vitro (Volkmer et al., 1998). Although the paranodal expression of Caspr and NF155 imply functions in axo-glial communication, the respective contribution of these molecules to the formation of the paranodal junction and their molecular interactions within the junctional complex remain elusive.

In this report, we identify contactin as a selective component of the paranodal axon membrane and reveal its novel and specific in vivo function in the assembly of the paranodal junction in the PNS. Contactin is a neural glycosylphosphatidylinositol (GPI)-anchored IgSF cell adhesion molecule (Ranscht and Dours, 1988; Brüm-

mendorf et al., 1989; Gennarini et al., 1989; Berglund and Ranscht, 1994) that can undergo *cis* and *trans* interactions with multiple proteins, including Caspr and NF155, respectively (Peles et al., 1997; Volkmer et al., 1998). Contactin is expressed on axons and dendrites of diverse neuron populations and, hence, is implicated in the development of neural circuitry. In vitro assays have recognized functions for contactin in neurite extension (Gennarini et al., 1991; Durbec et al., 1992; Peles et al., 1995), fasciculation (Chang et al., 1987; Rathjen et al., 1987), and repulsion (Pesheva et al., 1993). Mice with ablated contactin gene expression show neurological defects, including ataxia and hyperactivity, and display hindlimb weakness (Berglund et al., 1999). The mutation is lethal by postnatal day 18 (P18). Consistent with contactin's proposed role in neuronal circuitry formation, the ataxic phenotype is attributed, in part, to the disruption of contactin-mediated interactions by interneurons in the cerebellum (Berglund et al., 1999). Thus, contactin is a protein with established functions in neuron-neuron communication.

In the current study, we pursue the hindlimb weakness of the contactin mutants and explore the hypothesis that contactin contributes to the development and function of myelinated peripheral nerve. We report that contactin is a selective neuronal component of the paranode that regulates junctional attachment between axon and glial membranes. Contactin forms an intracellular complex with Caspr and enables its transport from the neuronal cell body to the axon membrane, where the complex accumulates at the paranode and engages in junction formation. Our data suggest that the contactin-Caspr complex communicates with paranodal myelin components, thereby orchestrating the junctional architecture that enables rapid conduction of nerve impulses.

Results

Disrupted Paranodal Axo-Glial Junction in Contactin Mutant Peripheral Nerve

To determine sites of contactin-mediated cellular interactions, we investigated the distribution of contactin in myelinating sciatic nerve. During the first 2 weeks of mouse postnatal development, contactin was dynamically redistributed from a uniform expression over the axon surface to a restricted localization at the paranode. Specifically, at P0, prior to ensheathment by premyelinating Schwann cells, contactin was expressed diffusely over the axolemma (Figure 1A). As Schwann cells engaged in the process of myelination, contactin progressively accumulated at the presumptive paranodal region (shown at P4 in Figure 1B). Clustering at the paranode became more pronounced as the myelin matured (shown at P14 in Figure 1C). In the adult myelinated nerve, contactin was confined to the paranodal axolemma (Figure 1D). Contactin was not detected on Schwann cells at any time postnatally. Thus, contactin is a selective component of the paranodal axolemma.

The propitious localization of contactin at the paranode raised the question if the lack of contactin expression affected myelination or axon-Schwann cell interactions. We utilized mice deficient for contactin gene expression to address this issue. Immunohistochemical analyses of P16 sciatic nerve revealed no overt differ-
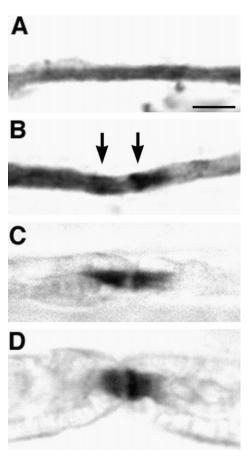

Figure 1. Developmental Profile of Contactin Expression in Myelinated Sciatic Nerve

(A) At P0, contactin is expressed diffusely along large caliber axons.

(B) By P4, contactin is in the process of redistributing to the paranodal region. The sites of presumptive paranodes are marked with arrows.

(C and D) From P14 (C) into adulthood (D), contactin is localized specifically at the paranode. Scale bar = 5 μm.

ences between genotypes in the distribution of myelin marker proteins CNP (2′3′-cyclic nucleotide 3′phosphohydrolase) and MAG (myelin-associated glycoprotein) (data not shown). To examine the fine structure of the myelin sheath, we performed ultrastructural analyses on spinal and sciatic nerves from wild-type and contactin mutant littermates at P14 and P16. Multiple myelin lamellae encircling individual axons were observed in transverse nerve sections in both genotypes (Figures 2A and 2B). The thickness of the myelin sheaths correlated with the axon diameter. Morphometric analysis showed that the g value (the ratio of axon diameter to fiber diameter) was within the normal range for myelinated axons in both genotypes (Table 1) (Little and Heath, 1994). Thus, the gross organization of myelin within contactin mutant mice was intact with respect to the periodic structure and the thickness of the myelin sheaths.

To investigate the nodal and paranodal region, we performed ultrastructural analyses on longitudinal sections of myelinated spinal and sciatic nerve at P14–P16. In both wild-type and contactin mutants, the nodal region was clearly discernable, between the flanking by the terminal myelin loops. In both genotypes, the para-
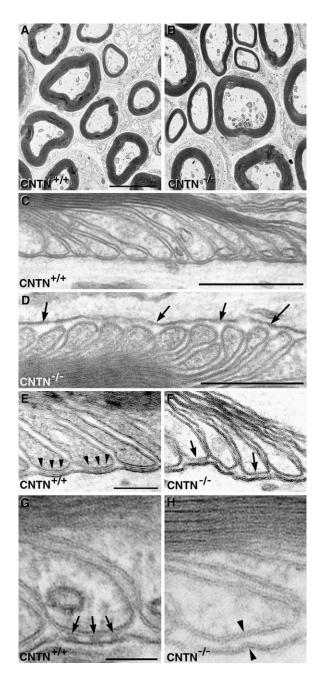
Figure 2. Ultrastructural Analysis Reveals Disrupted Paranodal Junctions in Peripheral Nerve

(A and B) Transverse sections of P16 wild-type (A) and mutant (B) sciatic nerve illustrate normal myelin profiles in both genotypes. Scale bar = 3.84 μm.

(C) In spinal nerve of P14 wild-type mice, the Schwann cell terminal loops are tightly attached to the axolemma at the paranode. Scale bar = 460 nm.

(D) Contactin mutant nerve shows loss of attachment at the paranodal junction in spinal nerve. Widened gaps between the terminal Schwann cell loops and the axolemma are marked with arrows. Scale bar = 288 nm.

(E and F) The axo-glial junction at the paranode in sciatic nerve of P16 wild-type (E) and contactin mutant (F) mice exhibit the same defect as in the spinal nerve. Scale bar = 115 nm.

(G and H) High magnification of spinal nerve at P14 shows the transverse bands (arrows) in the wild-type mice (G). In contrast, the transverse bands are absent in contactin mutant peripheral nerve (H). Scale bar = 57.5 nm.

Table 1. Morphometric Analysis of Contactin Mutant and Wild Type Peripheral Nerve

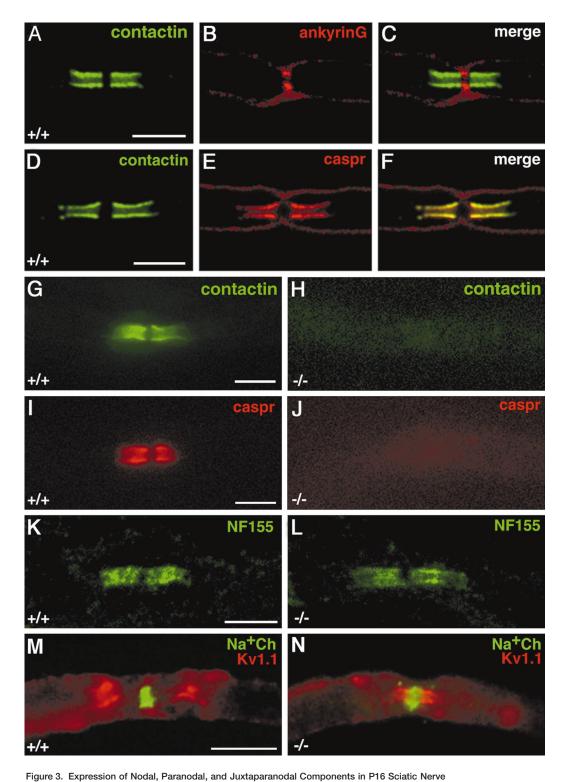| Parameter	+/+	−/−	p
Myelin (transverse)			
Axon diameter (μm)	1.94 ± 0.52	1.81 ± 0.57	0.0016
Fiber diameter (μm)	3.03 ± 0.91	2.69 ± 0.86	<0.0001
Ratio (g value)	0.66 ± 0.08	0.68 ± 0.08	<0.0001
Number of fibers	382	385	
Paranode (longitudinal)			
Gap + membrane (nm)	15.73 ± 0.80	20.43 ± 1.53	<0.0001
Number of nodes	5	8	

The ratio (g value = axon diameter/fiber diameter) reflects the extent to which fiber diameter is affected by axon diameter (Little and Heath, 1994). G values are within optimal range for maximal conduction velocity (Smith and Koles, 1970). Diameter measurements are given in micrometers. Distance measurements at the paranode show a significant increase of the gap between axonal and glial membranes in contactin mutants (−/−). Units are in nanometers and include the axolemma and the Schwann cell membrane, each with an average thickness of 5.11 nm. For each node, an average of 12 terminal loops were analyzed. Mean ± SD values are shown for all indicated parameters. A total of two animals for each genotype were used for morphometric analyses. Statistical analyses consisted of linear regression correlation and two-tailed Student's t test.

nodal myelin extended with the innermost lamella positioned furthest and the outermost lamella closest to the node. However, contactin mutant mice displayed a distinct defect in the attachment of the terminal myelin loops to the paranodal axolemma. The paranodal gap between the axolemma and the apposing myelin loops was significantly widened in the contactin mutant nerve (Figures 2C–2H). Morphometric measurements revealed an increase in the gap size from 5.51 nm in the wild-type to 10.21 nm in the mutant (corrected for membrane thickness; Table 1). Moreover, the electron dense transverse bands that are thought to represent sites of direct adhesive contact between the terminal myelin loops and the axolemma were absent in contactin mutants. These defects establish that contactin partakes in the formation of the septate-like axo-glial junctions at the paranode by regulating junctional attachment.

Mutant Paranodes Lack Caspr Expression
To gain insight into the molecular interactions of contactin in peripheral nerve, we first examined contactin expression in relation to nodal and paranodal proteins using immunohistochemical techniques. In P16 sciatic nerve, contactin staining was restricted to the paranode and was excluded from the nodes of Ranvier demarcated by sodium channels (data not shown) and the sodium channel binding protein ankyrin G (Figures 3A–3C). Double labeling for contactin and the paranodal protein Caspr revealed an overlapping staining pattern (Figures 3D–3F), suggesting that contactin and Caspr interact within the paranodal axon membrane.

We next explored the molecular rearrangements within perinodal membrane compartments in contactin mutants. Absence of contactin expression in mutant sciatic nerve confirmed that the mutation had effectively eliminated contactin gene expression (Figures 3G and 3H). In addition, Caspr expression at the paranode was abolished in absence of contactin (Figures 3I and 3J). Western blots revealed that Caspr protein was synthe-

Figure 3. Expression of Nodal, Paranodal, and Juxtaparanodal Components in P16 Sciatic Nerve

(A–C) Mutually exclusive distribution of contactin (A) and the nodal marker ankyrin G (B) demonstrates that contactin is not expressed at the node of Ranvier (C). (D–F) Double immunohistochemistry for contactin (D) and Caspr (E) shows overlapping expression at the paranode (F). (G and H) Contactin expression demarcates the paranodal region in wild-type sciatic nerve (G) but is absent in contactin mutants (H). (I and J) Caspr is localized at the paranode in wild-type nerve (I) but is not expressed in contactin mutant peripheral nerve (J). (K and L) Neurofascin 155 is expressed at the paranode in both wild-type (K) and contactin mutant mice (L). (M) Double labeling for sodium channels (green) and Kv1.1 (red) shows potassium channels at the juxtaparanodal region in wild-type nerve. (N) In contrast, the potassium channels are mislocalized to the paranode in contactin mutant nerve. Scale bar = 5 μm.
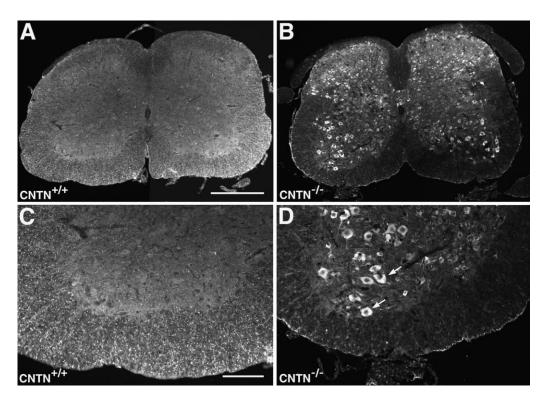
Figure 4. Aberrant Caspr Expression in the Soma of Motor Neurons

(A and C) In wild-type spinal cord, Caspr is expressed as paranodal clusters in the white matter. (B and D) In spinal cord from contactin mutant mice, Caspr staining is detected inside the cell bodies of large motor neurons. No staining is evident on nerve fibers in the white matter. Scale bar in (A) and (B) = 400 μm and in (C) and (D) = 50 μm.

sized within the CNS (data not shown). Hence, we explored the possibility that Caspr was retained within neuronal cell bodies in absence of contactin. To do that, we examined motor neuron somata and axons projecting into the peripheral nerve in transverse sections of the lumbar spinal cord. In the wild-type, Caspr staining was observed at the paranodes within the white matter (Figures 4A and 4C). In the mutants, Caspr was confined to the cell bodies of the large motor neurons located in the ventral horn (Figures 4B and 4D). These results show that Caspr was synthesized by motor neurons but was not transported to the axon membrane in absence of contactin. Thus, contactin and Caspr associate intracellularly, and contactin is necessary for the expression of the complex at the paranodal axon membrane.

The loss of paranodal attachment in the mutant suggests that the contactin-Caspr complex interacts with apposing myelin loops to form the septate-like junctions. An excellent candidate to engage in this interaction is NF155, a selective component of the paranodal myelin loops and a binding partner for contactin (Tait et al., 2000). To investigate if expression of NF155 is affected by the contactin mutation, we examined wild-type and contactin mutant sciatic nerve by immunohistochemistry. In both genotypes, we obtained staining for NF155 in the paranodal region (Figures 3K and 3L). However, in contrast to the robust paranodal NF155 expression in the wild-type, staining in the mutant was variable, and paranodal profiles were sometimes hard

to detect. We attribute this difference to the fact that the paranodal myelin loops are disengaged in contactin mutants, which in turn may destabilize expression of paranodal myelin components. Thus, expression of contactin is not necessary for localizing NF155 to the paranodal myelin loops, although contactin may partake in interactions with NF155 within the axo-glial junction.

Aberrant Localization of Shaker-Type Potassium Channels

Signals between axons and myelinating glial cells are suggested to cluster and position voltage-gated sodium channels to the node of Ranvier and potassium channels to the juxtaparanodal region underneath the myelin (Rasband et al., 1999; Vabnick et al., 1996). We used the contactin mutant mice to address if formation of the paranodal junction is a prerequisite for the clustering of voltage-gated ion channels in peripheral nerve. Immunohistochemistry for sodium channels demonstrated appropriate clustering to the narrow strip of the nodal axolemma in both genotypes (Figures 3M and 3N). Hence, the disruption of the paranodal junction did not affect the clustering of sodium channels at the node of Ranvier in myelinated peripheral nerve.

During development, potassium channels redistribute from a nodal and paranodal localization to delineate the juxtaparanodal region, a membrane domain adjacent to the paranode underneath the myelin sheath (Wang et al., 1993; Vabnick et al., 1999). Immunohistochemistry for the Shaker-type potassium channel subunits Kv1.1

and Kv1.2 revealed aberrant localization in P16 contactin mutant sciatic nerve (Figures 3M and 3N). While appropriate juxtaparanodal localization was observed in the wild-type, the Kv1.1 and Kv1.2 subunits were clustered at the paranode in contactin mutants. As contactin and potassium channel expression do not appear to overlap in the wild-type, we suggest that the aberrant potassium channel localization in the mutants is secondary to the disruption of the paranodal junction. Thus, paranodal attachment is critical for potassium channel translocation to the juxtaparanode, while the clustering of the sodium channels to the node of Ranvier is independent of contactin and junction formation in myelinated peripheral nerve.

Decreased Peripheral Nerve Conduction Velocity and Excitability

The results described above raise the question whether nerve function is compromised in contactin mutants. We addressed this issue in a series of electrophysiological experiments using the setup diagrammed in Figure 5A. To assess nerve conduction velocity, we analyzed compound action potentials (CAPs) in acutely isolated P16 sciatic nerve from both genotypes. We observed a 3-fold decrease of nerve conduction velocity in contactin mutant nerve as compared to the wild-type (Figures 5B and 5C). Moreover, we noted a dramatic difference between genotypes in the amount of voltage necessary to elicit a threshold response. For any given stimulus duration, the stimulus voltage required to evoke a minimum threshold response was 2.5 to 3 times higher for contactin mutant than for wild-type nerve (Figure 5D). These differences are consistent with changes in capacitance and resistance due to the loss of the paranodal axoglial junction (Chiu and Ritchie, 1980; Funch and Faber, 1984).

We were also interested in testing if the mislocalized Kv1.1 and Kv1.2 subunits in contactin mutants were able to contribute to spike repolarization (Chiu and Ritchie, 1984). Potassium channel function was assessed in P16 sciatic nerve by analyzing the refractory period using a paired-pulse stimulation protocol. The voltage of the stimulation was set at 80% of the maximal response. The first stimulus pair was delivered at a 10 ms interstimulus interval (ISI), with subsequent trials having shorter ISIs. With the gradual reduction of the ISI, the amplitude of the second CAP decreased in both genotypes. However, the amplitude decrease of the second CAP occurred sooner in the mutant than in the wild-type nerve (Figure 5E). When the mean amplitude of the second response relative to the first response was plotted as a function of the interstimulus interval, the mutant curve shifted to the right of the wild-type curve. These results indicate an increase of the refractory period in contactin mutant nerve (Figure 5F).

To determine specifically the contributions of the Kv1.1 and Kv1.2 channels to the repolarization of the resting potential, we analyzed the refractory period in the presence of dendrotoxin-I (DTX-I), a specific Kv1.1 and Kv1.2 potassium channel blocker (Dreyer and Penner, 1987; Zhou et al., 1998). DTX-1 had a modest effect on P16 wild-type sciatic nerve, as indicated by the slight shift of the repolarization curve to the right. However, in

the mutant, DTX-1 increased substantially the refractory period, as reflected by the significant rightward shift of the mutant curve (Figure 5F). The considerable difference in the refractory period between the DTX-1-treated and the untreated conditions suggests that the Kv1.1 and Kv1.2 potassium channels are functional and contribute to membrane repolarization in the mutant. We presume that DTX-1 is more efficacious in the mutant because the mislocalized channels are more accessible through the widened gap at the paranode.

Discussion

The formation of the specialized membrane domains in myelinated nerve requires a cascade of molecular signaling events between axons and glial cells. In the peripheral nervous system, Schwann cells establish a 1:1 relationship with axons and enwrap myelin around the axon segments between the presumptive nodes of Ranvier. As one of the final steps in myelinogenesis, the terminal myelin loops attach to the axon at the paranode and engage in the formation of the septate-like junctions. In this in vivo study, we have demonstrated that the GPI-linked cell adhesion molecule contactin organizes a molecular complex that confers junctional attachment between the axon and the myelin.

Formation of Paranodal Junctions Depends on Contactin-Mediated Signals

Contactin is the first GPI-linked membrane protein with a demonstrated function in junction formation. As it is anchored only to the outer leaflet of the plasma membrane, contactin must depend on interactions with laterally associated proteins to convey signals across the membrane. Consistent with their codistribution in myelinated peripheral nerve, contactin and Caspr form a *cis* complex within the paranodal axolemma. Formation of the contactin-Caspr complex is independent of myelin-inducing signals. Instead, the complex preforms intracellularly and depends on contactin-mediated signals for translocation to the cell surface. In the absence of contactin, Caspr is retained within neuronal cell bodies and is unavailable for interactions with membrane-associated components and extracellular ligands. Thus, the failure of Caspr to reach the axolemma in contactin mutants effectively eliminates all Caspr interactions at the cell surface. Our study therefore cannot discern the separate contributions of contactin and Caspr in paranodal membrane interactions. In agreement with our in vivo observations, a recent in vitro study also suggested that the cell surface expression of Caspr depends on contactin (Faivre-Sarrailh et al., 2000). In this report, Caspr was retained within the endoplasmic reticulum in singly transfected cells, while it was shuttled to the membrane in the presence of contactin. Our findings in contactin knockout mice extend significantly these in vitro observations by defining the paranodal region as one site where the contactin-Caspr complex plays an important functional role.

The paranodal defects in contactin mutants suggest that the contactin-Caspr complex engages in junctional attachment with molecules on the apposing glial membrane. So far, NF155 is the only myelin component
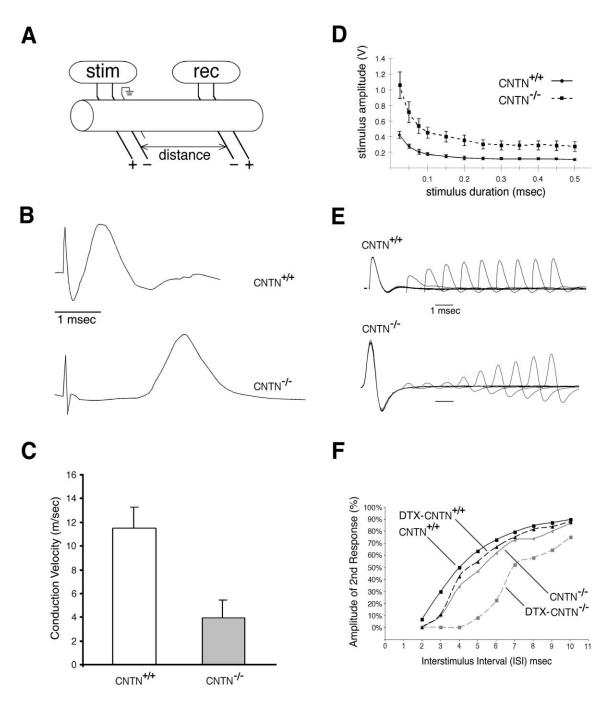
A

B

C

D

E

F

Figure 5. Electrophysiological Analysis of Sciatic Nerve

(A) Schematic showing arrangement of extracellular stimulation (stim) and recording (rec) electrodes. (B) CAPs recorded from wild-type ($CNTN^{+/+}$) and mutant ($CNTN^{-/-}$) P16 nerves. (C) Mean conduction velocity for $CNTN^{+/+}$ and $CNTN^{-/-}$ nerves. Variables are significantly different between wild-type and mutant (p < 0.0001, Student's t test; n = 6, $CNTN^{+/+}$; n = 9, $CNTN^{-/-}$). Error bars indicate standard deviation (SD). (D) Strength duration curves for $CNTN^{+/+}$ and $CNTN^{-/-}$ nerves. The voltage required to elicit a minimum threshold response is plotted for a given duration for both genotypes (n = 4, $CNTN^{+/+}$; n = 7, $CNTN^{-/-}$). Error bars indicate SD. (E) Paired-pulse stimuli at varying ISI were applied to study the refractory period in $CNTN^{+/+}$ and $CNTN^{-/-}$ nerves. Traces represent the maximal difference between the wild-type and mutant responses. (F) In refractory period experiments, the mean CAP amplitude of the second response relative to the first response is plotted as a function of ISI for both genotypes. The refractory periods are not significantly different between genotypes in the untreated condition. However, DTX-1 significantly reduces the refractory period in the mutant ($CNTN^{-/-}DTX$) as compared to the untreated mutant condition ($CNTN^{-/-}$) (p < 0.04, Student's t test). Moreover, a significant difference between DTX-1-treated mutant ($CNTN^{-/-}DTX$) and wild-type ($CNTN^{+/+}DTX$) nerves is observed (p < 0.02, Student's t test) (n = 7, $CNTN^{+/+}$ and $CNTN^{-/-}$; n = 2, $CNTN^{+/+}DTX$ and $CNTN^{-/-}DTX$). Error bars are standard error of the mean (SEM).
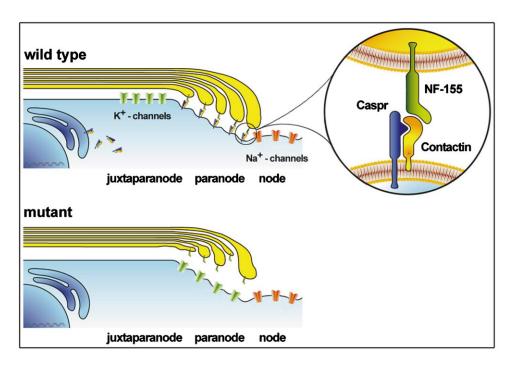
Figure 6. Model for Contactin Function at the Paranode

In the wild-type, contactin (yellow) associates intracellularly with Caspr (blue) and is necessary for translocating the complex to the paranodal axolemma, where it binds to NF155 (green) on the terminal myelin loops. Sodium channels (red) are clustered at the nodal region, and potassium channels (light green) are located in the juxtaparanodal region. In the mutants, the contactin-Caspr complex is not assembled; hence, Caspr is not expressed at the paranode. Although neurofascin is present on the paranodal myelin membrane, junctions do not form, as neurofascin cannot engage in interactions with the neuronal contactin-Caspr complex. In absence of the paranodal junction, sodium channels retain their nodal distribution, while potassium channels are aberrantly expressed at the paranodal region.

known to be selectively expressed at the paranode (Tait et al., 2000). There is evidence to suggest that the contactin-Caspr complex partakes in interactions with NF155. In vitro binding assays demonstrate that contactin and neurofascin can bind directly (Volkmer et al., 1998). Furthermore, the interaction between the contactin-Caspr complex and NF155 is indicated by studies in the *Shiverer* (*Shi*) mouse mutant. These mice carry a mutation which prevents the production of compact myelin and assembly of the paranodal axo-glial junction (Roach et al., 1985; Inoue et al., 1981; Rosenbluth, 1981). In *Shi* CNS white matter, clusters of Caspr and NF155 colocalize to ectopic sites, indicating an interaction between these molecules (Tait et al., 2000). In contactin mutants, NF155 is retained within the paranodal region, although the staining indicates a higher variability of expression than in the wild-type. From these data, we suggest that NF155 concentrates on the paranodal myelin loops independent of contactin-Caspr interactions. However, interactions with the contactin-Caspr complex within the paranodal junction appear to partake in stabilizing NF155 expression. This interaction may also play an important role in the junctional engagement between axons and glial cells.

We propose the following model for the molecular interactions at the paranode in myelinated peripheral nerve (Figure 6). Contactin engages in complex formation with the paranodal protein Caspr inside the cell and is necessary for transporting the complex to the axolemma. It remains to be determined whether the complex is intrinsically targeted to the paranode or if signals from myelinating Schwann cells induce paranodal clustering. At the paranode, the contactin-Caspr complex induces the formation of axo-glial junctions through interactions with the terminal Schwann cell loops. Our data indicate the direct role of the contactin-Caspr complex in the junctional attachment at the paranode. We suggest that interactions conferred by the contactin-Caspr complex stabilize NF155 expression on the paranodal myelin loops and hence contribute to junctional attachment. In contactin mutants, ablation of the contactin-Caspr complex results in the loss of junctional engagement at the paranode and leaves NF155 unoccupied.

In peripheral nerve, the mechanism controlling the clustering of sodium channels at the nodes of Ranvier appears to be independent of junctional adhesion at the paranode. In contactin mutants, sodium channels as well as ankyrin G clearly demarcate nodal regions of similar size and intensity as in the wild-type. This finding is in agreement with data from merosin (laminin $\alpha 2$)-deficient dystrophic mice (Deerinck et al., 1997). This mutation leaves nerves amyelinated and without glial cell contact, due to loss of Schwann proliferation and migration. Nevertheless, sodium channels cluster at the presumptive nodes of Ranvier, suggesting that the formation of the nodal specialization in peripheral nerve is controlled by factors other than Schwann cell junctional contact, including either intrinsic determinants or long-range diffusible factors.
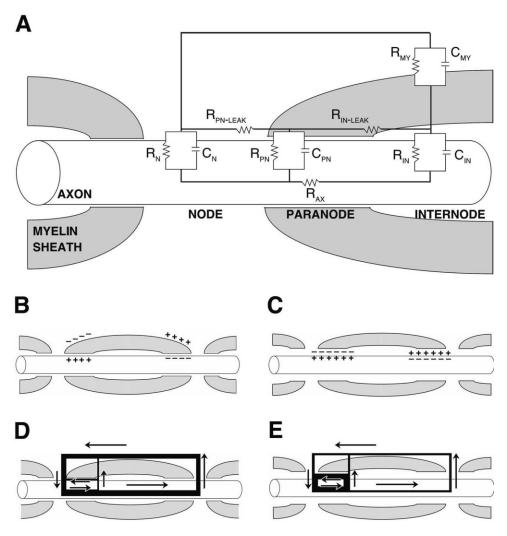
Figure 7. Model for Altered Physiology in Contactin Mutant Peripheral Nerve

(A) An equivalent circuit showing resistance and capacitance at the node (R_N and C_N), paranode (R_{PN} and C_{PN}), internode (R_{IN} and C_{IN}), and myelin (R_{MY} and C_{MY}). In addition to the axial resistance (R_{AX}), the leak resistances at the internode ($R_{IN-LEAK}$) and paranode ($R_{PN-LEAK}$) are depicted.
(B) Model for capacitance in wild-type myelinated axons.
(C) The loss of paranodal adhesion results in an increase in capacitance at the paranodal junction, due to the decreased distance between the intracellular and the extracellular compartments.
(D) Model for current flow in wild-type myelinated axons. Note that the majority of the axial current flows to the next node (depicted by the relative thickness of the lines drawn). A relatively small amount of current flows across the axonal membrane at the internode and completes the circuit by flowing radially through the myelin sheath or through the axo-glial junction at the paranode.
(E) In contactin mutant mice, we predict that the paranodal resistance is reduced due to the loss of adhesion between the Schwann cell terminal loops and the axolemma. This shift may lead to a proportionally large amount of current flowing back through the paranode instead of longitudinally through the axon and to the next node.

Formation of paranodal axo-glial junctions is a prerequisite for the juxtaparanodal positioning of the Shaker-class potassium channels (Rasband et al., 1998; Vabnick et al., 1999). The aberrant localization of potassium channels Kv1.1 and Kv1.2 to the paranode, rather than the juxtaparanode in contactin mutants, may therefore represent a secondary defect that is due to the loss of signaling at axo-glial junctions. Loss of contact at the paranode may eliminate a signal that triggers the developmental translocation of the potassium channels from the paranodal to the juxtaparanodal axon membrane and prevents the establishment or segregation of the juxtaparanodal membrane compartment.

Disrupted Paranodal Junctions Compromise Electrophysiological Properties of Peripheral Nerve

The ability to propagate action potentials via saltatory conduction relies critically upon the insulating function of myelin. Myelin reduces transmembrane resistive and capacitive currents in the paranodal and internodal regions. The electrical properties of the myelinated nerve depend on a number of parameters, including the ratio of fiber diameter to myelin thickness, the internodal distance, and the tightness of axo-glial contacts. Morphometric analyses of myelin in contactin mutants demonstrated that the ratio of axon diameter to total fiber diameter (g value) is within the optimal range for maximal

conduction velocity in both genotypes. In addition, initial analyses did not reveal an overt difference in internodal distance between genotypes (data not shown) (Brill et al., 1977). These data argue against myelin abnormalities that may reduce conduction velocity in contactin mutant nerves and suggest that the gross organization of myelinated axons, including axon diameter, myelin thickness, and internodal distance, is independent of contactin gene expression. Therefore, the disruption of the paranodal junction alone is likely to account for the impaired conduction velocity and reduced excitability observed in contactin mutant nerve.

The dramatic reduction in conduction velocity and the increase in voltage necessary to elicit threshold responses in contactin mutant sciatic nerve are consistent with changes in capacitive and resistive properties (Figure 7). Figure 7A represents a schematic of the electrical circuit in myelinated peripheral nerve, depicting the relative membrane resistive and capacitive contributions of the nodal, paranodal, and internodal compartments. Electrophysiological results presented in this paper predict an increase in capacitance at the paranode in contactin mutant mice. This observation is consistent with the report that disruption of the paranodal junction results in a 5-fold increase in the duration of the transient capacitive current (Figures 7B and 7C) (Chiu and Ritchie, 1980). In addition to this precipitous increase in paranodal capacitance, we predict that the specific resistance through the paranodal junction is decreased in contactin mutants (Figures 7D and 7E). This decrease may result in a radial shunting of internodal transmembrane current back through the paranode, thereby reducing the flow of longitudinal axoplasmic current to excite the downstream node (Barrett and Barrett, 1981; Funch and Faber, 1984) (Figure 7E). Our results thus support the view that the resistive and capacitive properties of the paranodal junction critically contribute to peripheral nerve physiology.

Paranodal Junctions with Respect to Myelin Function

The work presented in this paper highlights the importance of the septate-like axo-glial junctions at the paranode for the insulating function of myelin. Consistent with the hindlimb weakness of the contactin mutant mice, we suggest that the specific reduction of nerve conduction velocity and excitability decrease neuronal activity onto the target muscles, which in turn results in muscle atrophy. Phenotypically, the paranodal and physiological defects in myelinated contactin mutant peripheral nerve resemble those of mice mutant for UDP-galactose-ceramide galactosyltransferase (CGT) (Rosenbluth, 1980; Bosio et al., 1996; Coetzee et al., 1996). The CGT mutants lack the major and uniformly distributed myelin lipid constituents galactocerebroside and sulfatide. In the peripheral nervous system, these mutants also show the loss of the transverse bands and mislocalization of potassium channels at the paranodal region (Rosenbluth, 1980, 1981; Wang et al., 1995; Dupree et al., 1998, 1999; Dupree and Popko, 1999; Tait et al., 2000). However, the mechanism of how these glycolipids affect the formation of paranodal junctions remains less clear. One may speculate that changes in

lipid composition affect the expression or localization of paranodal myelin constituents and hence the interaction with axonal components in the formation of the septate-like junctions. Consistent with this suggestion, Caspr expression in the PNS is retained at the paranode of the CGT mutants, albeit staining is less intense (Dupree and Popko, 1999). Thus, it is conceivable that the contactin-Caspr complex is present in the paranodal region of the CGT mutants but cannot engage in junction formation, due to the loss of the corresponding glial ligand from apposing Schwann cell membranes. Based on this hypothesis, one may predict that myelin components directly involved in junctional adhesion at the paranode are lost in the CGT mutants. Future work will need to decipher the molecular link between the major myelin lipids and the assembly of the glial junctional complex at the paranode.

In sum, we have shown that contactin is critical for the assembly of a junctional complex that enables formation of the septate-like junctions between the paranodal axon membrane and the terminal Schwann cell loops in myelinated peripheral nerve. The axonal contactin-Caspr complex communicates with NF155 on paranodal Schwann cell membranes, either directly or through other proteins in a yet uncharacterized macromolecular adhesion/signaling complex. It remains to be determined if the function of contactin also applies to central myelinated nerve, where the pattern of contactin expression is more complex (E.O.B. and B.R., unpublished data) and the molecular interactions between axons and glial cells may depend on different molecular interactions than in the periphery. Elucidating the molecular signals that construct the septate-like axo-glial junctions and, specifically, the selective interactions of the contactin-Caspr complex will provide significant insights into the development, physiology, and pathology of this remarkable structure that enables rapid nerve impulse conduction.

Experimental Procedures

Derivation of Contactin-Deficient Mice
The derivation of mice homozygous for the mutant contactin allele has been described elsewhere (Berglund et al., 1999). In this study, a mixed line (129SVJ × C57Bl/6 × Black Swiss) and a purebred line (C57Bl/6) were used. Both lines display an identical phenotype (Berglund et al., 1999). In all experiments described in this paper, homozygous mutants were compared with wild-type littermates at postnatal day 16, unless otherwise noted.

Immunofluorescence and Immunohistochemistry
Three or more littermate pairs of wild-type and mutant mice were used in each experiment. For whole-mount staining of sciatic nerve, mice were sacrificed and the nerves dissected out in 0.1 M phosphate buffer. The nerves were teased and fixed for 30 min in 4% formaldehyde in 0.1 M phosphate buffer. For staining with anti-NF155, the nerves were fixed for an additional 15 min in Zamboni's fixative and teased onto slides. After several rinses in TBS, the nerves were blocked and permeabilized for 2 hr in 10% goat serum (Sternberger Monoclonals)/1% BSA (Sigma)/0.3% Triton X-100 (Tx-100; Sigma) in TBS at room temperature (RT) on a nutator. Nerves were incubated at 4°C for 24–48 hr in primary antibodies diluted in 3% goat serum/1% BSA/0.3% TX-100 in TBS. The following antibodies were used: affinity-purified rabbit anti-mCNTN-Ig1-6 (Berglund et al., 1999; 1:500–1:1000) mouse monoclonal and rabbit polyclonal antibodies to Caspr-1 (Peles et al., 1997; 1:200 and 1:2000); rabbit anti-NF155 (Tait et al., 2000; 1:100); mouse monoclonal anti-ankyrin

G (Zymed Laboratories, Inc.; 1:100); mouse monoclonal anti-Kv1.1 α subunit (Upstate Biotechnology; 1:100); mouse monoclonal anti-Kv1.2 (Upstate Biotechnology; 1:100); rabbit anti-sodium channel (loop III–IV; Upstate Biotechnology; 1:75); mouse monoclonal anti-2′3′-cyclic nucleotide 3′phosphohydrolase (CNP) (Promega; 1:750); and mouse monoclonal anti-myelin-associated glycoprotein (MAG) (Boehringer Mannheim; 1:30). Nerves were washed for 1 hr at room temperature in 0.1% TX-100 in TBS, before application of either fluorescently labeled (Molecular Probes) or biotinylated (Vector) secondary antibodies. Nerves with fluorescent secondary antibody were washed in 0.1% Tx-100 in TBS, mounted in SlowFade Light (Molecular Probes), and analyzed with a Nikon Inverted microscope or a BioRad MRC1024-MP confocal laser scanning system. Nerves incubated with biotinylated secondary antibodies were washed in TBS, incubated with ABC tertiary complex (Vector), and washed in TBS. After development in the DAB substrate solution (0.05% DAB, 0.01% H_2O_2 in Tris), the nerves were mounted and analyzed with a Nikon Eclipse TE300 microscope.

For immunofluorescence of cryosections, mice were anesthetized with Avertin (Aldrich) and transcardially perfused with a vascular rinse of 0.9% NaCl followed by 4% formaldehyde in 0.1 M phosphate buffer. Spinal cords were dissected and cryoprotected in 25% sucrose in 0.1 M phosphate buffer overnight at 4°C. After embedding in O.C.T. compound (Sakura Finetek), spinal cords were cryosectioned at 15 μm and collected in phosphate-buffered saline (PBS). Floating sections were rinsed in TBS and blocked with 5% goat serum in TBST (0.1% Tx-100 in TBS) for 1 hr at room temperature. Sections were incubated at 4°C for 24 hr in primary antibody (anti-Caspr; 1:1000) diluted in antibody solution (TBST with 5% goat serum/0.1% Tx-100). Sections were washed in TBST and then incubated for 1 hr at room temperature with goat anti-rabbit Alexa 488-conjugated secondary antibodies (Molecular Probes; 1:300). For examination, sections were coverslipped and viewed on an inverted Nikon Eclipse-TE300 microscope.

Standard Electron Microscopy

Preparations for standard electron microscopy were as previously described (Friedrich and Mugnaini, 1981). Sections of sciatic nerve or spinal nerve from the brachial plexa were either longitudinally sectioned for examining the paranodal formations or transversely to study the myelin wrapping. Ultrathin sections were collected on 200 mesh grids and photographed with a Hitachi 600 electron microscope.

Quantification of Paranodal Loop Gaps and Myelin Wraps

Ultrathin longitudinal sections of sciatic nerve were examined in two sets of mutant and wild-type pairs of mice. Electron micrographs of nodes of Ranvier were taken at 100,000× magnification, scanned, and digitized in NIH Image. The gap between the axonal surface and the center of each paranodal loop was measured as a straight line from the inner leaflet of the axon membrane to the inner leaflet of the opposing glial cell membrane (n = 75 wild-type, and n = 118 knockout). No overt difference in the thickness of axon and glia membranes was observed between genotypes. The distances obtained from mutant mice were compared to those from wild-type littermates by an unpaired, two-tailed Student's t test.

For quantification of myelin wraps and axonal diameters, ultrathin transverse sections of sciatic nerve were examined in two sets of mutant and wild-type pairs of mice. Electron micrographs were taken at the center of each nerve at 3000× magnification, scanned, and digitized in NIH Image. The axonal area of individual nerves was measured after thresholding the image, and the diameter was calculated. The myelin sheet was measured as the shortest distance across the wraps (n = 332 wild-type, and n = 385 knockout). Data were evaluated statistically, using an unpaired, two-tailed Student's t test and regression analyses.

Electrophysiological Analyses

Conduction and repolarization properties of myelinated axons were examined in acutely isolated sciatic nerves from P16 contactin mutant and wild-type mice shown in Figure 5. The nerves were pinned down in a Sylgard® dish and recorded with Ag-AgCl electrodes arranged according to the schematic diagramed in Figure 5A. The

electrodes were electrically isolated with Vaseline®. The proximal end of the nerve was stimulated, and the distal end was used to record the compound action potential (CAP). The preparation was superfused with oxygenated Krebs' solution, as described in Coetzee et al. (1996). All recordings were conducted at room temperature.

Conduction velocity was determined by the difference in conduction delay of the stimulus peak artifact to the peak of the compound action potential (CAP). The distance parameter was calculated as the distance from the negative stimulating electrode to the negative recording. The DTX-I (Calbiochem) blocker was added directly to the Krebs solution to yield the appropriate dilution (1 μM). CAPs were amplified, digitized, recorded, and analyzed using Scope 3.3 software using MacLab hardware.

References

Barrett, E.F., and Barrett, J.N. (1981). Intracellular recording from vertebrate myelinated axons: mechanism of the depolarizing afterpotential. J. Physiol. *323*, 117–144.

Berglund, E.O., and Ranscht, B. (1994). Molecular cloning and in situ localization of the human contactin gene (CNTN1) on chromosome 12q11-q12. Genomics *21*, 571–582.

Berglund, E.O., Murai, K.K., Fredette, B., Sekerkova, G., Marturano, B., Weber, L., Mugnaini, E., and Ranscht, B. (1999). Ataxia and abnormal cerebellar microorganization in mice with ablated contactin gene expression. Neuron *24*, 739–750.

Bosio, A., Binczek, E., and Stoffel, W. (1996). Functional breakdown of the lipid bilayer of the myelin membrane in central and peripheral nervous system by disrupted galactocerebroside synthesis. PNAS USA *93*, 13280–13285.

Bostock, H., and Sears, T.A. (1978). The internodal axon membrane: electrical excitability and continuous conduction in segmental demyelination. J. Physiol. *280*, 273–301.

Brill, M.H., Waxman, S.G., Moore, J.W., and Joyner, R.W. (1977). Conduction velocity and spike configuration in myelinated fibres: computed dependence on internode distance. J. Neurol. Psychiatry *40*, 769–774.

Brümmendorf, T., Wolff, J.M., Frank, R., and Rathjen, F.G. (1989). Neural cell recognition molecule F11: homology with fibronectin type III and immunoglobulin type C domains. Neuron *2*, 1351–1361.

Chang, S., Rathjen, F.G., and Raper, J.A. (1987). Extension of neurites on axons is impaired by antibodies against specific neural cell surface glycoproteins. J. Cell Biol. *104*, 355–362.

Chiu, S.Y., and Ritchie, J.M. (1980). Potassium channels in nodal and internodal axonal membrane of mammalian myelinated fibres. Nature *284*, 170–171.

Chiu, S.Y., and Ritchie, J.M. (1984). On the physiological role of internodal potassium channels and the security of conduction in myelinated nerve fibers. Proc. R. Soc. Lond. B *220*, 415–422.

Coetzee, T., Fujita, N., Dupree, J., Shi, R., Blight, A., Suzuki, K., Suzuki, K., and Popko, B. (1996). Myelination in the absence of

galactocerebroside and sulfatide: Normal structure with abnormal function and regional instability. Cell 86, 209–219.

Deerinck, T.J., Levinson, S.R., Bennett, G.V., and Ellisman, M.H. (1997). Clustering of voltage-sensitive sodium channels on axons is independent of direct Schwann cell contact in the dystrophic mouse. J. Neurosci. 17, 5080–5088.

Dreyer, F., and Penner, R. (1987). The actions of presynaptic snake toxins on membrane currents of mouse motor nerve terminals. J. Physiol. 386, 455–463.

Dupree, J.L., and Popko, B. (1999). Genetic dissection of myelin galactolipid function. J. Neurocytol. 28, 271–279.

Dupree, J.L., Coetzee, T., Blight, A., Suzuki, K., and Popko, B. (1998). Myelin galactolipids are essential for proper node of Ranvier formation in the CNS. J. Neurosci. 18, 1642–1649.

Dupree, J.L., Girault, J.-A., and Popko, B. (1999). Axo-glial interactions regulate the localization of axonal paranodal proteins. J. Cell Biol. 147, 1145–1151.

Durbec, P., Gennarini, G., Goridis, C., and Rougon, G. (1992). A soluble form of the F3 neuronal cell adhesion molecule promotes neurite outgrowth. J. Cell Biol. 117, 877–887.

Einheber, S., Zanazzi, G., Ching, W., Scherer, S., Milner, T.A., Peles, E., and Salzer, J.L. (1997). The axonal membrane protein Caspr, a homologue of Neurexin IV, is a component of the septate-like paranodal junctions that assemble during myelination. J. Cell Biol. 139, 1495–1506.

Ellisman, M.H., Wiley, C.A., Lindsey, J.D., and Wurtz, C.C. (1984). Structure and function of the cytoskeleton and endomembrane systems at the node of Ranvier. In The Node of Ranvier. Cellular Neurobiology, J.C. Zagoren and S. Fedoroff, eds. (Orlando, FL: Academic Press, Inc.), pp. 153-181.

Faivre-Sarrailh, C., Gauthier, F., Denisenko-Nehrbass, N., Le Bivic, A., Rougon, G., and Girault, J.A. (2000). The glycosylphosphatidyl inositol-anchored adhesion molecule F3/contactin is required for surface transport of paranodin/contactin-associated protein (caspr). J. Cell Biol. 149, 491–502.

Friedrich, V.L., and Mugnaini, E. (1981). Preparation of neural tissues for electron microscopy. In Neuroanatomical Tract-Tracing Methods, L. Heimer and M.J. Robards, eds. (New York, Plenum Press), pp. 345–375.

Funch, P.G., and Faber, D.S. (1984). Measurement of myelin sheath resistances: Implications for axonal conduction and pathophysiology. Science 225, 538–540.

Gennarini, G., Cibelli, G., Rougon, G., Mattei, M.G., and Goridis, C. (1989). The mouse neuronal cell surface protein F3: a phosphatidylinositol-anchored member of the immunoglobulin superfamily related to chicken contactin. J. Cell Biol. 109, 775–788.

Gennarini, G., Durbec, P., Boned, A., Rougon, G., and Goridis, C. (1991). Transfected F3/F11 neuronal cell surface protein mediates intercellular adhesion and promotes neurite outgrowth. Neuron 6, 595–606.

Inoue, Y., Nakamura, R., Mikoshiba, K., and Tsukada, Y. (1981). Fine structure of the central myelin sheath in the myelin deficient mutant Shiverer mouse, with special reference to the pattern of myelin formation by oligodendroglia. Brain Res. 219, 85–94.

Kaplan, M.R., Meyer-Franke, A., Lambert, S., Bennett, V., Duncan, I.D., Levinson, S.R., and Barres, B.A. (1997). Induction of sodium channel clustering by oligodendrocytes. Nature 386, 724–728.

Lambert, S., Davis, J.Q., and Bennett, V. (1997). Morphogenesis of the node of Ranvier: Co-clusters of ankyrin and ankyrin-binding integral proteins define early developmental intermediates. J. Neurosci. 17, 7025–7036.

Little, G.J., and Heath, J.W. (1994). Morphometric analysis of axons myelinated during adult life in the mouse superior cervical ganglion. J. Anat. 184, 387–398.

Menegoz, M., Gaspar, P., Le Bert, M., Galvez, T., Burgaya, F., Palfrey, C., Ezan, P., Arnos, F., and Girault, J.A. (1997). Paranodin, a glycoprotein of neuronal paranodal membranes. Neuron 19, 319–331.

Peles, E., and Salzer, J.L. (2000). Molecular domains of myelinated axons. Curr. Opin. Neurobiol. 10, 558–565.

Peles, E., Nativ, M., Campbell, P.L., Sakurai, T., Martinez, R., Lev, S., Clary, D.O., Schilling, J., Barnes, G., and Schlessinger, J. (1995). The carbonic anhydrase domain of receptor tyrosine phosphatase β is a functional ligand for the axonal cell recognition molecule contactin. Cell 82, 251–260.

Peles, E., Nativ, M., Lustig, M., Grumet, M., Schilling, J., Martinez, R., Plowman, G.D., and Schlessinger, J. (1997). Identification of a novel contactin-associated transmembrane receptor with multiple domains implicated in protein-protein interactions. EMBO J. 16, 978–988.

Pesheva, P., Gennarini, G., Goridis, C., and Schachner, M. (1993). The F3/11 cell adhesion molecule mediates the repulsion of neurons by the extracellular matrix glycoprotein J1–160/180. Neuron 10, 69–82.

Ranscht, B., and Dours, M.T. (1988). Sequence of contactin, a 130-kD glycoprotein concentrated in areas of interneuronal contact, defines a new member of the immunoglobulin supergene family in the nervous system. J. Cell Biol. 107, 1561–1573.

Rasband, M.N., Trimmer, J.S., Schwarz, T.L., Levinson, S.R., Ellisman, M.H., Schachner, M., and Shrager, P. (1998). Potassium channel distribution, clustering, and function in remyelinating rat axons. J. Neurosci. 18, 36–47.

Rasband, M.N., Peles, E., Trimmer, J.S., Levinson, S.R., Lux, S.E., and Shrager, P. (1999). Dependence of nodal sodium channel clustering on paranodal axoglial contact in the developing CNS. J. Neurosci. 19, 7516–7528.

Rathjen, F.G., Wolff, J.M., Frank, R., Bonhoeffer, F., and Rutishauser, U. (1987). Membrane glycoproteins involved in neurite fasciculation. J. Cell Biol. 104, 343–353.

Roach, A., Takahashi, N., Pravtcheva, D., Ruddle, F., and Hood, L. (1985). Chromosomal mapping of mouse myelin basic protein gene and structure and transcription of the partially deleted gene in Shiverer mutant mice. Cell 42, 149–155.

Rosenbluth, J. (1980). Peripheral myelin in the mouse mutant shiverer. J. Comp. Neurol. 193, 729–740.

Rosenbluth, J. (1981). Axoglial junctions in the mouse mutant shiverer. Brain Res. 208, 283–297.

Rosenbluth, J. (1984). Membrane specializations at the nodes of Ranvier and paranodal and juxtaparanodal regions of myelinated central and peripheral nerve fibers. In The Node of Ranvier. Cellular Neurobiology, J.C. Zagoren and S. Fedoroff, eds. (Orlando, FL: Academic Press, Inc.), pp. 31–67.

Rosenbluth, J. (1987). Abnormal axoglial junctions in the myelin-deficient rat mutant. J. Neurocytol. 16, 497–509.

Rosenbluth, J. (1995). Glial membranes and axoglial junctions. In Neuroglia, H. Kettenmann and B.R. Ransom, eds. (New York, Oxford University Press), pp. 613–633.

Salzer, J.L. (1997). Clustering sodium channels at the node of Ranvier: Close encounters of the axon-glia kind. Neuron 18, 843–846.

Smith, R.S., and Koles, Z.J. (1970). Myelinated nerve fibers: computed effect of myelin thickness on conduction velocity. Am. J. Physiol. 219, 1256–1258.

Tait, S., Gunn-Moore, F., Collinson, J.M., Huang, J., Lubetzki, C., Pedraza, L., Sherman, D.L., Colman, D.R., and Borphy, P.J. (2000). An oligodendrocyte cell adhesion molecule at the site of assembly of the paranodal axo-glial junction. J. Cell Biol. 150, 657–666.

Trapp, B., and Kidd, G.J. (2000). Axo-glial septate junctions: The maestro of nodal formation and myelination? J. Cell Biol. 150, F97–F99.

Vabnick, I., Novakovic, S.D., Levinson, S.R., Schachner, M., and Shrager, P. (1996). The clustering of axonal sodium channels during development of the peripheral nervous system. J. Neurosci. 16, 4914–4922.

Vabnick, I., Trimmer, J.S., Schwarz, T.L., Levinson, S.R., Risal, D., and Shrager, P. (1999). Dynamic potassium channel distributions during axonal development prevent aberrant firing patterns. J. Neurosci. 19, 747–758.

Volkmer, H., Zacharias, U., Norenberg, U., and Rathjen, F.G. (1998). Dissection of complex molecular interactions of neurofascin with

axonin-1, F11, and tenascin-R, which promote attachment and neurite formation of tectal cells. J. Cell Biol. *142*, 1083–1093.

Wang, H., Kunkel, D.D., Martin, T.M., Schwartzkroin, P.A., and Tempel, B.L. (1993). Heteromultimeric K^+ channels in terminal and juxtaparanodal regions of neurons. Nature *365*, 75–79.

Wang, H., Allen, M.L., Grigg, J.J., Noebels, J.L., and Tempel, B.L. (1995). Hypomyelination alters K^+ channel expression in mouse mutants shiverer and Trembler. Neuron *15*, 1337–1347.

Wiley, C.A., and Ellisman, M.H. (1980). Rows of dimeric-particles within the axolemma and juxtaposed particles within glia, incorporated into a new model for the paranodal glial-axonal junction at the node of Ranvier. J. Cell Biol. *84*, 261–280.

Zhou, L., Zhang, C.L., Messing, A., and Chiu, S.Y. (1998). Temperature-sensitive neuromuscular transmission in Kv1.1 null mice: role of potassium channels under the myelin sheath in young nerves. J. Neurosci. *18*, 7200–7215.